Quantitative evaluation of particle pinning force on a grain boundary using the phase-field method

2012 Modelling Simul. Mater. Sci. Eng. 20 055004

(http://iopscience.iop.org/0965-0393/20/5/055004)

Modelling Simul. Mater. Sci. Eng. **20** (2012) 055004 (11pp) doi:10.1088/0965-0393/20/5/055004

Quantitative evaluation of particle pinning force on a grain boundary using the phase-field method

Kunok Chang[1] **and Long-Qing Chen**

Department of Materials Science and Engineering, The Pennsylvania State University, University Park, PA 16802, USA

E-mail: ferromag@gmail.com

Received 11 October 2011, in final form 8 May 2012
Published 13 June 2012
Online at stacks.iop.org/MSMSE/20/055004

Abstract

Second-phase particles are often employed to inhibit the grain growth of polycrystalline materials. We studied the interaction between a second-phase particle and a grain boundary using the phase-field method. In particular, we determined the magnitude of pinning force exerted by a particle on a grain boundary. We considered the effect of particle morphology by examining several particle shapes including spherical, ellipsoidal and cubic. The pinning forces computed from the phase-field were compared with available analytical theories for spherical and ellipsoidal particle shapes. We derived an expression for the pinning force of a grain boundary by a cubic particle and compared the prediction with phase-field simulations. The present results should be useful for evaluating the effect of particle morphology on the effectiveness of grain growth inhibition by second-phase particles.

(Some figures may appear in colour only in the online journal)

1. Introduction

Zener derived the pinning force of a grain boundary by a single second-phase particle [1]. In his derivation, he assumed that the interface between a particle and matrix is always incoherent and the shape of the second-phase particle is spherical [1]. However, the shape of the second-phase particle in reality can be rather complicated, varying from being spherical to needle-shaped [2, 3], plate-like [3, 4] or cuboidal [3, 5–9]. Ashby *et al* incorporated the effect of coherent interface on the particle pinning force [10]. Ryum *et al* [11] and Nes *et al* [12] extended the Zener theory to an ellipsoidal particle and considered the intersection of a grain boundary at a right angle with a second-phase particle. Easterling *et al* proposed a numerical method to

[1] Author to whom any correspondence should be addressed.

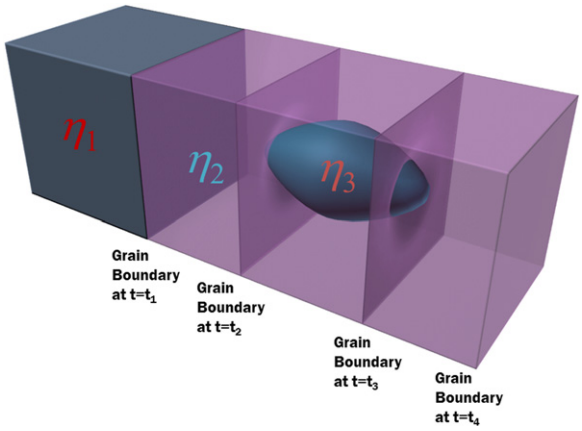

Figure 1. This is a schematic drawing of a system set-up to study the interaction between a grain boundary and a particle. We introduced two order parameters (η_1, η_2) to indicate the different orientations of the two grains. The third order parameter (η_3) represents the second-phase particle. To move the grain boundary, the driving force (ξ) is added in the free energy in equation (3).

calculate the pinning force by an ellipsoidal particle intersecting with a grain boundary along any arbitrary angle [13]. The Zener pinning effect has been studied using various types of computational methods including the phase-field method in 2D [14–17], the finite element method [18, 19], the vertex model [18, 20] and the Monte Carlo Potts model [18, 21]. In this study, we employed the phase-field method to determine the pinning force of a grain boundary by a second-phase particle. The main advantage of the phase-field approach is the possibility to consider any arbitrary shapes of a particle, multi-particles, and any configuration of a grain boundary. However, to quantify the pinning force, we will focus on the interaction between a single particle and a single grain boundary. We evaluate the pinning force for several simple particle shapes including sphere [1] as well as ellipsoid which meets a boundary under the right angle [11, 12]. This allows us to compare the results from the phase-field simulations to the predictions of analytic theories proposed by Zener [1] and Ryum *et al* [11] Nes *et al* [12]. To the best of our knowledge, the pinning force on a grain boundary by a cuboidal second-phase particle has not been evaluated. Therefore, we quantitatively estimated the pinning force of a cuboidal particle on a grain boundary and compare the results with phase-field simulations. For simplicity, the degree of interfacial coherency between matrix and a second-phase particle is not considered.

2. Phase-field model of particle/grain boundary interaction

We designed a simple system made up of a grain boundary and a second-phase particle in figure 1. To describe a grain boundary in figure 1, we introduced two order parameters (η_1, η_2) to indicate the different orientations of the two grains. A third order parameter (η_3) is introduced to represent a second-phase particle. While we assume η_3 is static, representing an inert particle, we move the grain boundary by solving the following time-dependent equations for η_1, η_2 [14–17, 22, 23]:

$$\frac{\partial \eta_i}{\partial t} = -M_i \left(\frac{\delta F}{\delta \eta_i} \right), \qquad i = 1, 2, \tag{1}$$

where M_i denote grain boundary mobilities and F the total free energy of the system. In the simulations, we assumed identical, constant values for all M_i. The free energy is a function of the order parameters and their gradients [14–17, 22, 23]:

$$F = \int_V \left[f_0(\eta_1, \eta_2, \eta_3) + \frac{1}{2} \sum_{i=1}^{2} \kappa_i (\nabla \eta_i)^2 \right] \mathrm{d}V, \tag{2}$$

where f_0 represents a local free energy density and the κ_i are gradient energy coefficients. We choose the function f_0 to have degenerate minima. A simple function f_0 satisfying this requirement is given by

$$f_0(\eta_1, \eta_2, \eta_3) = \sum_{i=1}^{2} \left(-\frac{1}{2}\alpha \eta_i^2 + \frac{1}{4}\beta \eta_i^4 \right) + \gamma \sum_{i=1}^{2} \sum_{j=1}^{3} \eta_i^2 \eta_j^2 + \xi \eta_1, \tag{3}$$

where α, β and γ are phenomenological constants [14–17, 22, 23]. Substitution of equations (2) and (3) into equation (1) yields the equation of motion,

$$\frac{\partial \eta_i}{\partial t} = -M_i \left(-\alpha_i \eta_i + \beta_i \eta_i^3 + 2\gamma_i \eta_i \sum_{j \neq i}^{3} \eta_j^2 - \kappa_i \nabla^2 \eta_i + \xi \phi_i \right), \tag{4}$$

where ξ is the driving force for grain boundary movement and $\phi_1 = 1$ and $\phi_2 = 0$.

Equation (4) is solved using a simple forward-Euler integration scheme [14–17, 22, 23]. We assumed that the grain boundary mobility and energy are isotropic. All parameters used in the phase-field model are given in non-dimensional units. The system size is $100 \times 100 \times 100$, and we choose $\Delta x = 1.0$. A periodic boundary condition is applied along the x- and y-directions. However, we assumed that $\eta(z = 0) = \eta(z = \Delta x)$and $\eta(z = 101\Delta x) = \eta(z = 100\Delta x)$ as boundary conditions. We examined the effect of this boundary condition along the z-direction on the grain boundary morphology and the pinning force, we found that the effect was not notable. The coefficients in equation (4) were chosen as follows: $\alpha_i = \beta_i = \gamma_i = 1$, $\kappa_i = 2$ and $M_i = 1$ for all i. The time step Δt was set to 0.05.

3. Pinning force evaluation

When a grain boundary is entirely arrested by a second-phase particle, the driving force for grain boundary migration is balanced by a capillarity force of a curved grain boundary [9]. To determine the maximum driving force ($\xi_{\max}$) which maintains the pinned state of the grain boundary, we increase ξ in equations (3) and (4) in steps of $\Delta\xi = 10^{-5}$. Since the grain boundary in the phase-field modeling is diffuse [14–16, 21, 22], we needed to determine the grain boundary location to accurately evaluate the driving force. We used the order parameter *isosurface* ($\eta_1 = 0.5$) in Matlab to extract the corresponding sharp interface position of the grain boundary, and the obtained sharp grain boundary configuration is visualized in figure 1 as the red curved surface). The output of the *isosurface* routine in Matlab (figure 2) is an array listing vertices comprising each triangle and the other array containing the coordinates of each of these vertices. Armed with this list of triangles and their coordinates, we can easily calculate the face area ($\mathrm{d}A$) and surface normal unit vector ($\hat{n}$). In equations (3) and (4), we apply the driving force to move the grain boundary along the direction normal to the isosurface. The pinning forces along the x- and y-direction are canceled out due to their geometrical symmetry. Therefore, the particle pinning force is given as follows:

$$F_{\mathrm{p}} = \xi_{\max} \int \hat{n} \cdot \hat{z} \, \mathrm{d}A = \xi_{\max} \Phi. \tag{5}$$

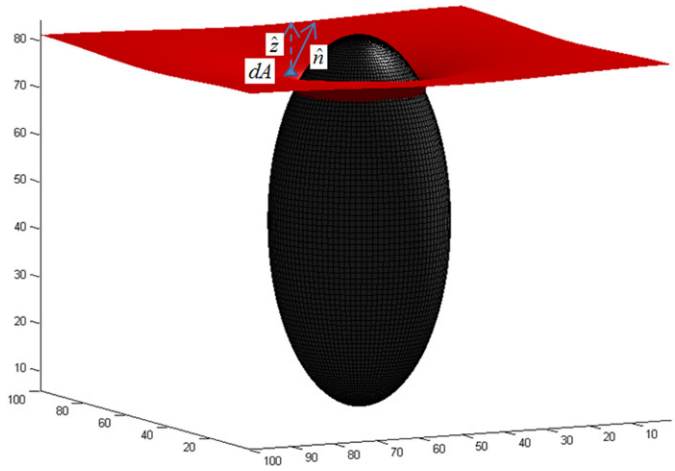

Figure 2. The grain boundary pinned by a second-phase particle. The applied driving force (ξ) for grain boundary movement is $\xi_{\max}$. The sharp grain boundary (red curved plane) is determined by *isosurface* subroutine in *Matlab* with the linear interpolation flag. The gray ellipsoid is the second-phase particle and its equation is $((x-50)^2/19.2^2)+((y-50)^2/19.2^2)+((z-45)^2/39.3^2)=1$. The grain boundary is visualized by *patch* command in *Matlab* and the ellipsoid is visualized by *ellipsoid* command. dA represents a small area comprising three vertices, and the normal unit vector ($\hat{n}$) is determined by vertices coordinates.

4. Pinning forces by spherical and ellipsoidal particles

The analytic relations of the particle pinning force were derived by Zener [1] for a spherical particle and by Ryum *et al* [11] and Nes *et al* [12] for an ellipsoidal particle. Zener and Ryum *et al* and Nes *et al* assumed that the interfacial energy between matrix and second-phase particle is isotropic [1, 11, 12]. Also, Ryum *et al* [11] and Nes *et al* [12] only considered the situation that a second-phase particle meets a grain boundary at the right angle. Zener derived the following relation [1]:

$$F_{\mathrm{p}} = \pi r \sigma_{\mathrm{gb}}, \tag{6}$$

where σ_{gb} is the grain boundary energy and $r$is a spherical particle radius. In our simulation, the non-dimensional grain boundary energy σ_{gb} is 0.536. We compared the pinning forces calculated from equations (5) and (6) in figure 3. We found that Zener's theory shows overall good agreement with our phase-field simulation; the differences at a given particle radius (r) is less than 6%.

Figure 4 is an illustration of two cases of interactions between a grain boundary and a second-phase particle considered by Ryum *et al* [11] and Nes *et al* [12]. The pinning force for case I is derived analytically [11, 12] and given by [11, 12]:

$$F_{\mathrm{p}} = F_{\mathrm{p}}^{\mathrm{S}} \frac{2}{(1+\varepsilon)\varepsilon^{1/3}}, \tag{7}$$

where $F_{\mathrm{p}}^{\mathrm{S}}$ is the pinning force of a same-volume spherical particle and $\varepsilon = b/a$ is the eccentricity of the ellipsoidal particle [11, 12].

We compared equations (5) and (7) for ellipsoidal particles with different eccentricities in figure 5. Couturier *et al* also showed that the oblate particle is more effective in particle pinning in case I compared with the same-volume spherical or prolate particle [24] and this prediction is consistent with our simulation result.

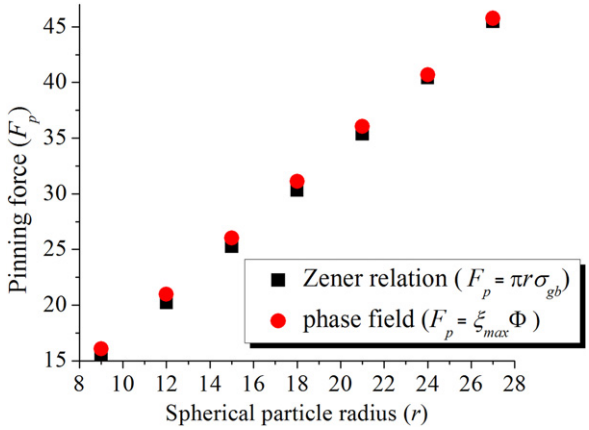

Figure 3. The pinning forces calculated from the Zener's theory [1] (equation (6)) are plotted using black squares, and the pinning forces calculated from the phase-field simulation (equation (5)) are plotted using red circles. The difference between two pinning forces at given particle radius (r) is at most 6%.

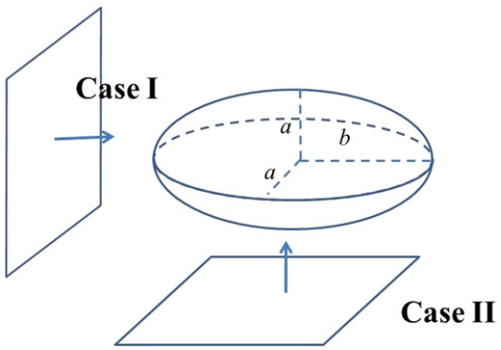

Figure 4. Schematic illustration of two cases of particle–grain boundary interaction in [11, 12]. Ryum *et al* and Nes *et al* only considered the cases when a boundary meets a particle under the right angle. The illustration is re-drawn by current authors.

In case II, Ryum *et al* and Nes *et al* estimated the pinning force numerically [11, 12]:

$$F_{\mathrm{p}} = \sigma_{\mathrm{gb}} \int \cos\theta \, \mathrm{d}l \tag{8}$$

and $\cos\theta$ and $\mathrm{d}l$ are given as follows [11, 12]:

$$\cos\theta = \left\{ \left(\frac{\partial x}{\partial y}\right)^2 + \left(\frac{\partial x}{\partial z}\right)^2 + 1 \right\}^{-1/2}, \tag{9}$$

$$\mathrm{d}l = \left\{ 1 + \left(\frac{\partial z}{\partial y}\right)^2 \right\}^{1/2} \mathrm{d}y. \tag{10}$$

Ryum *et al* [11] and Nes *et al* [12] assumed that a second-phase particle makes a planar hole on the grain boundary. They fitted the curve from the numerical integration piecewise, and

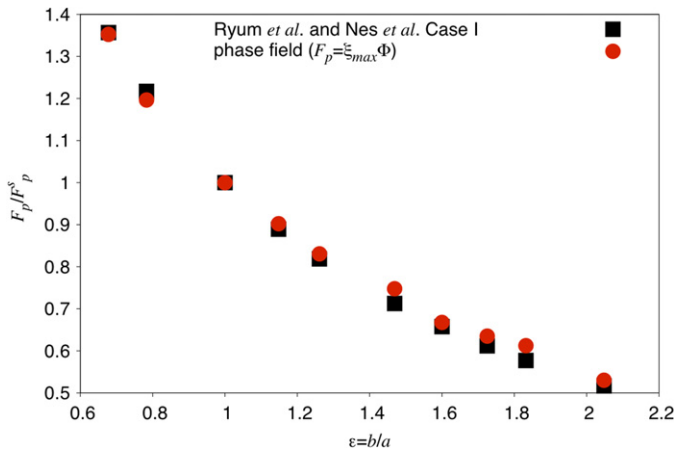

Figure 5. The pinning forces calculated from Ryum *et al* and Nes *et al*'s expression [11, 12] (equation (7)) are plotted using black squares, and the pinning forces calculated from the phase-field simulation (equation (5)) by red circle. The volumes of all particles are identical but the eccentricities are different. The difference between two pinning forces from equation (7) and equation (5) at a given eccentricity (ε) is at most 5%.

their results are given as follows [11, 12]:

$$F_{\mathrm{p}} = F_{\mathrm{p}}^{\mathrm{S}} \frac{(1 + 2.14\varepsilon)}{\pi \varepsilon^{1/2}} \qquad \text{when } \varepsilon \geqslant 1,$$
$$F_{\mathrm{p}} = F_{\mathrm{p}}^{\mathrm{S}} \varepsilon^{0.47} \qquad \text{when } \varepsilon < 1. \tag{11}$$

Based on the comparison of phase-field simulation results and equation (11), we found that equation (11) is not very accurate. Therefore, we propose a new fitting function (equation (12)) for the pinning force for case II,

$$F_{\mathrm{p}} = F_{\mathrm{p}}^{\mathrm{S}}(5.04 - 4.38\mathrm{e}^{-\varepsilon/11.58} - 0.40\mathrm{e}^{-\varepsilon/0.35}) \qquad \text{when } (0.30 \leqslant \varepsilon \leqslant 4.63). \tag{12}$$

We assumed that the eccentricity of ellipsoidal particle ranges from 0.3 to 4.63. Results from equations (8), (11) and (12) are plotted in figure 6. The agreement between equations (8) and (12) is much better than the that between equations (8) and (11) especially when the eccentricity (ε) is larger than 1.

The agreement between the phase-field simulation and Ryum *et al* and Nes *et al*'s theory is fairly good for case II (equation (12)) (figure 7). Also, we found that the newly constructed fitting function in this work shows better agreement compared with the Ryum *et al* and Nes *et al*'s fitting function (equation (11)).

5. Pinning force by a cuboidal particle

Cuboidal precipitates are quite common for cubic precipitates in a cubic matrix, e.g., gamma-prime precipitates in the Ni-alloy matrix in Ni-based superalloys [3, 5–9]. Easterling *et al* already evaluated the pinning force applied by a cuboidal particle using the theoretical approach [25]. We performed phase-field simulations to measure pinning forces applied by a cuboidal particles, and the results will be compared with the analytic theory. In this paper, we introduced three assumptions:

(1) The interface energy between the matrix and the particle is isotropic;

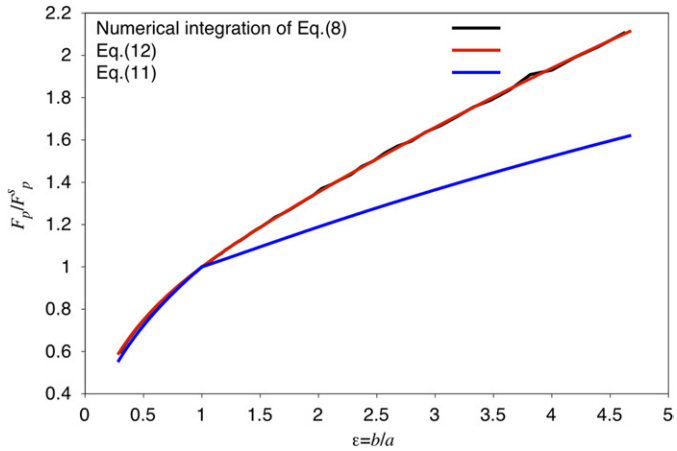

Figure 6. F_p/F_p^s curves from the equations (8), (12) and (11). The black curve is obtained from equation (8) numerically. Equation (11) (blue curve) is the fitted function of F_p/F_p^s in [11]. Equation (12) (red curve) is the new fitted function of F_p/F_p^s for $0.30 \leqslant \varepsilon \leqslant 4.63$. The agreement between the red and black curves is significantly better than that between the blue and black curves for $\varepsilon > 1$.

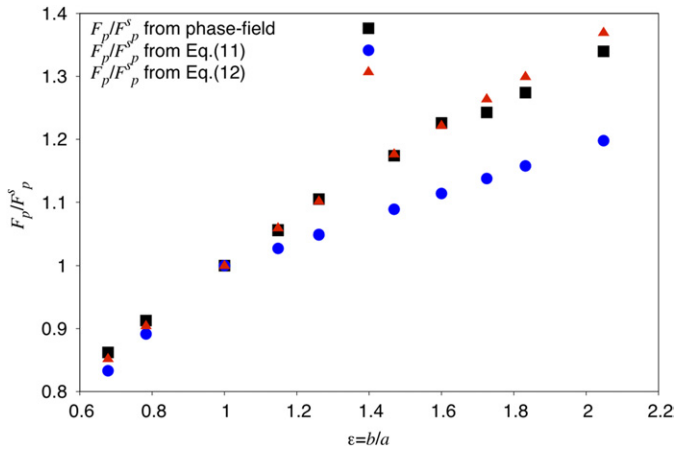

Figure 7. F_p/F_p^s curves from the phase-field modeling and equations (11) and (12) for case II in figure 4. Equation (12) (red triangles) is the new fitted function of F_p/F_p^s in this work, showing significantly improved agreement compared with the equation (11) (blue circles) by Ryum *et al* and Nes *et al* [11, 12].

(2) A grain boundary meets a second-phase particle at the right angle;
(3) The particle makes sharp-cornered square hole on the grain boundary.

With the above three assumptions, we derived the cuboidal particle dragging force in figure 8 as follows:

$$F_p = \sigma_{gb} \times (2c + 2d) \times \cos 45^\circ = \sqrt{2}(c + d)\sigma_{gb}. \tag{13}$$

We compared the pinning force by a cubic (edge length $c = d = e$) with that of a sphere (radius r) with the same volume in equation (14). Since $V = c^3 = (4\pi/3)r^3$,

$$F_p^{cubic} = 2\sqrt{2}c\sigma_{gb} = 2\sqrt{2}\sqrt[3]{\frac{4\pi}{3}}r\sigma_{gb}, \tag{14}$$

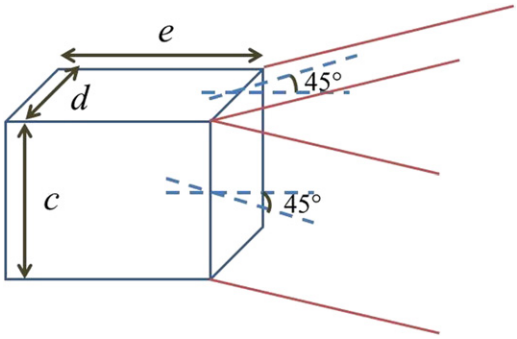

Figure 8. The grain boundary (red line) pinned by a cuboidal particle (blue line). The edge lengths of the cuboid are c, d and e. Since the interface energy between matrix and particle is isotropic, the dihedral angle between grain boundary and the cuboid face is 45°.

where $F_{\mathrm{p}}^{\mathrm{c}}$ is the cubic particle Zener force. The pinning force by a spherical particle ($F_{\mathrm{p}}^{\mathrm{s}}$) is given in equation (6). Therefore,

$$F_{\mathrm{p}}^{\mathrm{cubic}} = 2\sqrt{2}c\sigma_{\mathrm{gb}} = 2\sqrt{2}\sqrt[3]{\frac{4\pi}{3}}r\sigma_{\mathrm{gb}} \approx 1.45F_{\mathrm{p}}^{\mathrm{sphere}}. \tag{15}$$

To examine the accuracy of equation (13), we introduced one cuboidal particle in a simulation. The edge lengths are given as $c = 39$, $d = 39$ and $e = 38$. The pinning forces from equation (13) and (5) are 59.13 and 61.95, respectively. The dragging force from equation (5) was approximately 4.8% higher than the force from equation (13), and this discrepancy is higher than that of the spherical particle case; the difference between the dragging forces from equation (5) and (13) is smaller than 0.6%. The cuboidal particle and the captured grain boundary are visualized in figures 9(a) and (b). As shown in figures 9(a) and (b), the hole on the grain boundary is round-cornered rather than sharp-cornered right-angle rectangle. Therefore, the fourth assumption we made is not strictly true in phase-field simulations. Therefore, it is understandable that the pinning forces from equations (5) and equation (13) for the cuboidal particle are slightly different.

The thermodynamic driving force for particle pinning is the reduction in the grain boundary area. Therefore, the particle pinning force increases with the increase in the area of the hole on the grain boundary. We found that the hole develops rounded corners in our simulations. According to Cahn and Hilliard [26], there is a contribution of the gradient energy to the interfacial energy. If the hole is a square with sharp corners, the gradient energy goes to infinity at the corners. Consequently, the square with rounded corners is more favorable than one with sharp corners for pinning the motion of grain boundary.

According to equation (13), the dragging force does not depend on the length of edge (c) which lies along the z direction (direction of grain boundary movement). To validate this result, we measured the dragging forces of three rectangular cuboids with $c = d = 39$ and $e = 38, 25, 12$. The pinning force of three rectangular cuboids from equation (13) is the same value of 59.13, and force from equation (5) is 61.95 regardless e values.

Indeed, the particle pinning force does not depend on the edge length c according to table 1. The result is consistent with the analytic theory given by equation (13).

Zener force increases as the hole area on the grain boundary ($A = cd$) increases according to table 1.

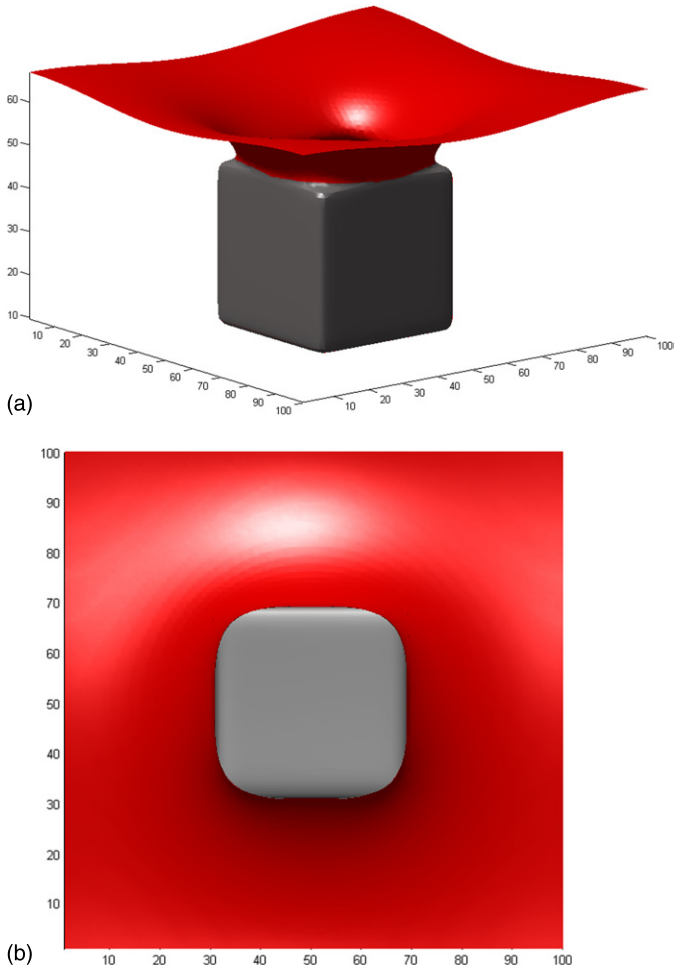

Figure 9. The grain boundary (red plane) pinned by the rectangular cuboids (grey cubic). (a) side view (b) top view. The hole on the grain boundary is rounded-corner in (a) and (b).

Table 1. Particle dragging forces applied by three rectangular cuboids. The lengths of three edges c, d and e in figure 8 are given in the table. The dragging forces from equations (13) and (5) increased as the hole area on the grain boundary ($A = cd$) increased.

c	d	e	F_p (equation (13))	F_p (equation (5))
33	33	38	50.03	51.91
39	39	38	59.13	61.95
45	45	38	68.22	70.91

6. Comparing effectiveness of grain growth inhibition

In order to compare the effectiveness of grain growth retardation by spherical, ellipsoidal and cuboidal particles, we introduced four assumptions:

(1) The volume of particle is the same;
(2) A grain boundary meets a particle under a right angle;

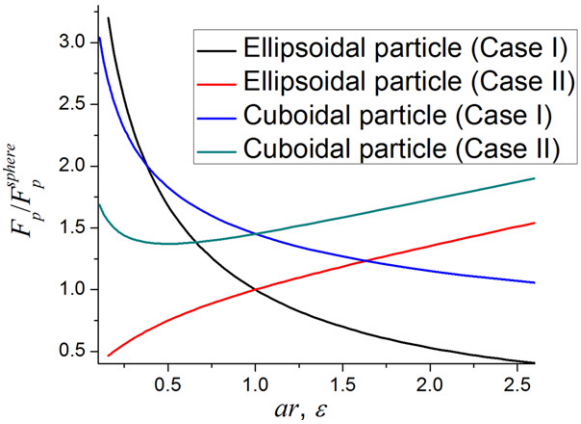

Figure 10. F_p/F_p^s curves of ellipsoidal particle for case I (black curve) of ellipsoidal particle, case II (red curve) of ellipsoidal particle, case I of cuboidal particle (blue curve) and case II of cuboidal particle (green curve). We assumed that the grain boundary meets a particle under a right angle and edge lengths c and d of the cuboidal particle in figure 8 are same. Aspect ratio (ar) of the cuboidal particle is given by e/c and the eccentricity (ε) of the ellipsoidal particle is given by b/a. The definition of length a and $b$is described in figure 4.

(3) $c = d$ in figure 8;
(4) The aspect ratio of the cuboidal particle (ar $= c/e$) is introduced. The pinning force of the cuboidal particle is compared with the force of the ellipsoidal particle when $ar = \varepsilon$ (aspect ratio of the cuboidal particle = eccentricity of the ellipsoidal particle).

The key factor in determining pinned average grain size is the maximum pinning force [1, 11]. In figure 10, the maximum driving force by an ellipsoidal particle arise in case I when $\varepsilon < 1$. If $\varepsilon > 1$, the maximum driving force is obtained from case II. We found that when the aspect ratio or the eccentricity is larger than 0.35, the ellipsoidal particle is more effective in pinning rather than the cuboidal particle. However, the aspect ratio or the eccentricity is below 0.35, the cuboidal particle is more effective in pinning. In addition, we compared the ratio of distances crossed by the dragging phase and driving phase for the spherical particle ($\varepsilon = 1$) and the cubic particle (ar $= 1$). We found that the ratio of cubic particle (2.0) is higher than that of spherical particle (1.3). Therefore, the cubic particle is more effective in particle pinning comparing with the spherical particle in our study.

7. Conclusion

We performed phase-field simulations to quantitatively measure the interaction between a second-phase particle and a grain boundary. We found that Zener's theory for the spherical particle and Ryum *et al* and Nes *et al*'s theory for an ellipsoidal particle when the particle meets a grain boundary under the right angle predict pinning forces which are in good agreement with results from phase-field simulations. We derived the expression for the pinning force of a grain boundary by a cubic particle with an assumption that the particle makes the square hole on the grain boundary. The pinning forces calculated from the expression are slightly different from the pinning forces from the phase-field simulations. This difference can be attributed to the rounded corners of the square hole arising from the phase-field simulations. We found that when the aspect ratio or the eccentricity is larger than 0.35, the ellipsoidal particle is

more effective in pinning rather than a cuboidal particle while when the aspect ratio or the eccentricity is below 0.35, the cuboidal particle is more effective in pinning.

We are presently employing phase-field simulations to evaluate the particle pinning force under more realistic condition taking into account coherency for the particle-matrix interface as well as the Zener force by an ellipsoidal second-phase particle intersecting with a grain boundary along any arbitrary angle.

Acknowledgments

The authors acknowledge financial support from the National Science Foundation (grant number DMR-0710483) and CCMD (Center for Computational Materials Design). Computing time was provided on instrumentation funded by the National Science Foundation through grant OCI-0821527. The authors also thank Dr Saswata Bhattacharya for useful comments and Yongha Hwang for helping with the illustrations.

References

[1] Smith C 1948 *Trans. Am. Inst. Min. Metall. Eng.* **175** 15
[2] O'Bryan H and Thomson J 1983 *J. Am. Ceram. Soc.* **66** 66
[3] Ardell A and Nicholson R 1966 *J. Phys. Chem. Solids* **27** 1793
[4] Song H and Coble R 1990 *J. Am. Ceram. Soc.* **73** 2086
[5] Goken M and Kempf M 1999 *Acta Mater.* **47** 1043
[6] Chen Z, Lorretto M and Cochrane R 1987 *Mater. Sci. Technol.* **3** 836
[7] Sireesha M, Shankar V, Albert S and Sundaresan S 2000 *Mater. Sci. Eng.* A **292** 74
[8] Christopher B M, Zugang M, Noebe R D and Seidman D N 2008 *Appl. Phys. Lett.* **93** 033103
[9] Nathal M V, MacKay R A and Miner R V 1989 *Metall. Mater. Trans.* A **20** 133
[10] Ashby M, Harper J and Lewis J 1969 *Trans. Metall. Soc. AIME* **245** 413
[11] Ryum N, Hunderi O and Nes E 1983 *Scr. Mater.* **17** 1281
[12] Nes E, Ryum N and Hunderi O 1985 *Acta Metall.* **33** 11
[13] Li W and Easterling E 1990 *Acta Metall.* **38** 1045
[14] Moelans N, Blanpain B and Wollants P 2006 *Acta Mater.* **54** 1175
[15] Chang K, Feng W and Chen L Q 2009 *Acta Mater.* **57** 5229
[16] Moelans N, Blanpain B and Wollants P 2007 *Acta Mater.* **55** 2173
[17] Suwa Y, Saito Y and Onodera H 2006 *Scr. Mater.* **55** 407
[18] Miodownik M A 2002 *Model Light Met.* **2** 125
[19] Couturier G, Doherty R, Maurice C and Fortunier R 2005 *Acta Mater.* **53** 977
[20] Weygand D, Brechet Y and Lepinoux J 1999 *Acta Mater.* **47** 961
[21] Kad B K and Hazzledine P M 1997 *Mater. Sci. Eng.* A **238** 70
[22] Chen L Q and Yang W 1994 *Phys. Rev.* B **50** 15752
[23] Krill C E III and Chen L Q 2002 *Acta Mater.* **50** 3057
[24] Couturier G, Fortunier R and Maurice C l 2000 *Proc. 21st Riso Int. Symp. on Materials Science (Roskilde, Denmark)* p 303
[25] Ringer S P, Li W and Easterling E 1989 *Acta Metall.* **37** 831
[26] Cahn J W and Hilliard J E 1958 *J. Chem. Phys.* **28** 258